la402012d

DATASET · JUNE 2014

READS
25

6 AUTHORS, INCLUDING:

Weijin Li
Fujian Institute of Research on the Structure o…
10 PUBLICATIONS **73** CITATIONS
SEE PROFILE

Shuiying Gao
Chinese Academy of Sciences
49 PUBLICATIONS **810** CITATIONS
SEE PROFILE

Langmuir

Article

pubs.acs.org/Langmuir

In Situ Growth of Metal–Organic Framework Thin Films with Gas Sensing and Molecule Storage Properties

Wei-Jin Li,[†,‡] Shui-Ying Gao,[†] Tian-Fu Liu,[†] Li-Wei Han,[†] Zu-Jin Lin,[†] and Rong Cao*[,†]

[†]State Key Laboratory of Structural Chemistry, Fujian Institute of Research on the Structure of Matter, Chinese Academy of Science, 350002 Fuzhou, People's Republic of China

[‡]University of Chinese Academy of Science, 100049 Beijing, People's Republic of China

Supporting Information

ABSTRACT: New porous metal–organic framework (MOF) films based on the flexible ligand 1,3,5-tris[4-(carboxyphenyl)oxamethyl]-2,4,6-trimethylbenzene (H_3TBTC) were fabricated on α-Al_2O_3 substrates under solvent thermal conditions. The factors affecting the fabrication of films, such as the temperature of pre-activation and the dosage of the reagents, were investigated. Tuning the subtle factors on film fabrications, a series of MOF thin films with different morphologies and grain sizes were prepared. The morphology and grain size of the films are monitored by scanning electron microscopy (SEM). X-ray diffraction (XRD) and attenuated total reflection infrared (ATR–IR) were also used to characterize the MOF films. The results indicate that the temperature of pre-activation and the dosage of the reagents are the key parameters during the process of film formation. The properties of the films, especially the sensing and sorption behavior, have been studied by an optical digital cameral and ultraviolet–visible (UV–vis) spectra. The evidence shows that the films are sensitive to small organic molecules, such as methanol and pyridine. Meanwhile, the films can adsorb small dye molecules. Thus, the films may have potential applications in either organic vapor sensing or storage of small dye molecules.

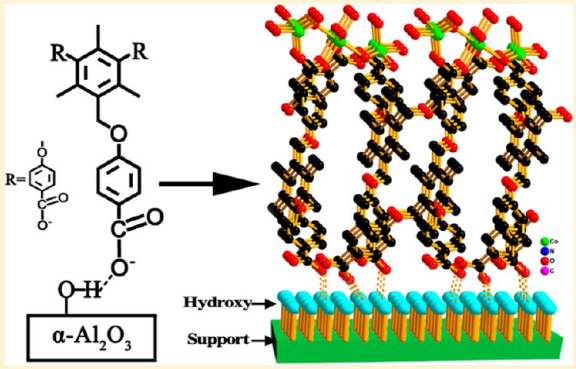

1. INTRODUCTION

In the last few decades, metal–organic frameworks (MOFs) have attracted tremendous attention, owing to their potential applications in catalysis, molecular sensing, gas storage and separation, etc.[1−4] Meanwhile, many scientists devote much interest to explore functional films, such as non-porous hybrid films[5−8] and porous crystalline films.[9−15] Recently, porous MOF-based films have increasingly become a popular research topic because the MOF films can be manipulated into devices and their properties are similar to bulk crystal materials. To the best of our knowledge, fabrication of the first crystalline and porous film was a zeolite membrane, which was successfully deposited on various supports.[9−11] Nevertheless, difficulties in functionalizing the pores of zeolites and controlling the properties of the films have greatly limited their further applications. In this context, the multifunctional MOF materials may overcome these limitations. Subsequently, MOF-5[12−15] (with $[Zn_4O(bdc)_4]$ cluster units) and HKUST-1[16−20] (with $[Cu_3(btc)_2]$ cluster units) films have been thoroughly studied. More recently, other MOF films, such as the MIL series, have also been reported.[21−24] Ongoing research in this field has been mostly focused on the fabrication of MOF films constructed by simple building units and rigid organic ligands.

As far as we know, the crystalline porous MOF films based on flexible organic ligands have not yet been reported. In comparison to rigid ligands, flexible ligands exhibit plentiful peculiarities. First, the flexibility of these ligands helps to form the MOFs with particular structures and properties,[25−27] such as molecular switch derived from a conformational change, the "breathing" ability in the solid state, adaptive recognition property for coexisting guests or counterions, and flexible molecular clips composed of prismatic coordination discrete molecules. Then, MOFs constructed by flexible ligands may change their structures and properties reversibly in response to external stimulus. This behavior can be significant for sensor applications. However, it would be difficult to prepare the MOF films based on flexible ligands, because flexible ligands can adopt different conformations and low symmetry as a result of the rotations of single bonds. In addition, the structures based on flexible ligands are more sensitive to many subtle factors, and the growth conditions should be controlled strictly. Our group has long been focusing on the research of MOF materials with flexible ligands.[28−31] A series of MOFs/coordination polymers (CPs) based on flexible ligands, such as tetrakis[4-(carboxyphenyl)oxamethyl] methane acid (H_4X) and tetrakis-[(3,5-dicarboxyphenoxy)-methyl]methane) (H_8X), were synthesized. Looking into the series of H_4X and H_8X, the flexible $-O-CH_2-$ moieties endow the ligands certain flexibility and effectively decrease the steric hindrance between the phenyl

Received: February 21, 2013
Published: June 7, 2013

   dx.doi.org/10.1021/la402012d | *Langmuir* 2013, 29, 8657–8664

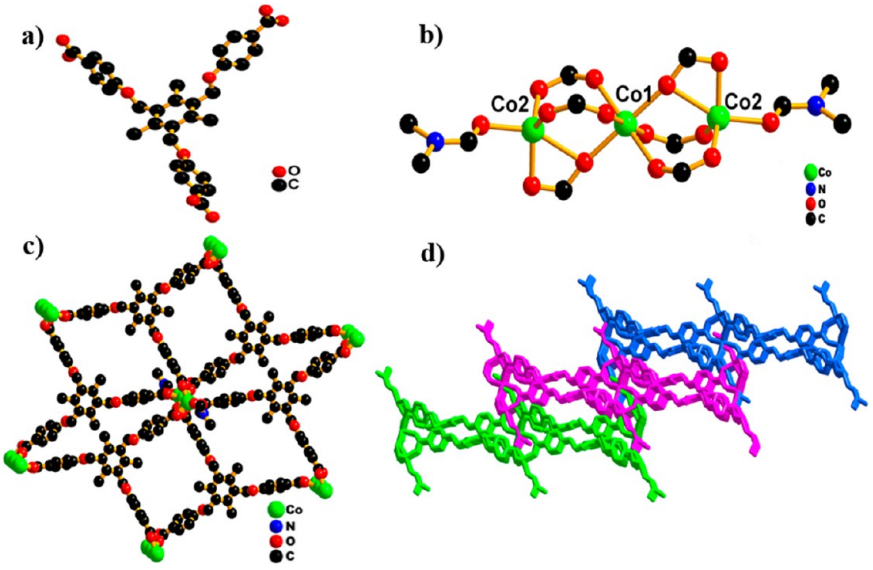

Figure 1. Simplified representation of the geometry of the ligand in the compound and crystal: (a) H_3TBTC ligand, (b) trimetallic cluster in compound **1**, (c) three-connected $TBTC^{3-}$ ligand link clusters in the 2D layer, and (d) 2D layer stack in the 3D framework.

units. Inspired by the aforementioned work, we aim at fabricating the MOFs constructed by flexible ligands onto the solid surfaces.

Herein, new porous MOF films based on the flexible ligand 1,3,5-tris[4-(carboxyphenyl)oxamethyl]-2,4,6-trimethylbenzene (H_3TBTC) were fabricated on α-Al_2O_3 substrates under solvent thermal conditions. The MOF compound formulated as $[Co_3(TBTC)_2{\cdot}(DMF)_2]{\cdot}4DMF$ (**1**) has also been characterized herein. When subtle factors are tuning on film fabrication, the MOF films can display various particular morphologies and grain sizes. Thus, the temperature of preactivation and the dosage of the reagents were extensively investigated. In addition, the flexibility of the ligand may leave the porous films with good ability of molecular sensing. Furthermore, the porous MOF films based on H_3TBTC may possess good capacities to store and transport small organic molecules. The optical digital camera and ultraviolet−visible (UV−vis) spectrum were used to confirm characteristic behaviors.

2. EXPERIMENTAL SECTION

2.1. Materials. 1,3,5-Tris(bromomethyl)-2,4,6-trimethylbenzene was purchased from TCI, and ethyl-*p*-hydroxybenzoate and $Co(NO_3)_2{\cdot}6H_2O$ were purchased from Sinopharm Chemical Reagent Beijing Co., Ltd. They were all used without further purification. All reagents and solvents were commercially available and used as received. Ultrapure water (18.24 MΩ cm^{-1}) is used directly from a Milli-Q water system. Porous α-Al_2O_3 ceramic disks (diameter of 20 mm and thickness of 0.7 mm with double side polished) were purchased from Hefei Kejing Materials Technology Co., Ltd. (China).

2.2. Methods. X-ray diffraction (XRD) patterns of the films were collected on a Panalytical X'pert Pro MPD diffractometer using graphite-monchromated Co Kα radiation in the 2θ range of 5−30° with a step size of 0.02°. The scanning electron microscopy (SEM) measurement was carried out on a JEOL JSM-6700F instrument. Attenuated total reflection infrared (ATR−IR) spectra of the samples were measured using a Nicolet 6700 Fourier transform infrared (FTIR) spectrometer with an ATR sampling accessory. The ATR cell was made of a horizontal ZnSe crystal with an incidence angle of 45°. The optical photos were obtained from a Canon Digital IXUS 9901S camera. UV−vis absorption spectra were recorded on Shimadzu UV-2550 (Japan). Elemental analyses of the bulk powders were carried out on an Elementar Vario EL III analyzer. Thermogravimetric analysis (TGA) of the bulk powders was performed under nitrogen at a scan rate of 10 °C/min using TA STDQ600 instruments. The nitrogen adsorption experiment was performed at 77 K on a Micromeritics ASAP 2020 sorption analyzer. Infrared spectra of the bulk powders were measured from KBr pellets using PerkinElmer Spectrum One. ^1H nuclear magnetic resonance (NMR) spectra were recorded at ambient temperature on a BRUKER AVANCE III spectrometer.

2.3. Synthesis of $[Co_3(TBTC)_2(DMF)_2]{\cdot}4DMF$. $Co(NO_3)_2{\cdot}6H_2O$ (**1**) (0.2 mmol, 58 mg) and H_3TBTC[32] (0.1 mmol, 57 mg) were dissolved in a mixture of 10 mL of 4:1:1 (volume ratio) DMF/EtOH/H_2O by strong stirring for 10 min at room temperature. Then, the solution was poured into the Teflon-lined stainless-steel vessel (23 mL). After heating under autogenous pressure at 120 °C for 72 h, the Teflon-lined stainless-steel vessel was slowly cooled to room temperature at a constant rate of 0.04 °C min^{-1}. The deep blue crystals of compound **1** were obtained and dried in air at ambient temperature. Yield: 53% (on the basis of H_3TBTC). Analytical elementary analysis calculated (%) for $C_{84}H_{92}Co_3N_6O_{24}$: C, 57.77; H, 5.31; N, 4.81%. Found: C, 56.58; H, 5.35; N, 4.46%. IR (KBr): 3434 (s), 3078 (vw), 2927 (v), 1681 (s), 1657 (s), 1605 (vs), 1560 (m), 1509 (w), 1385 (vs), 1306 (w), 1243 (s), 1177 (m), 1145 (w), 1106 (w), 1085 (w), 989 (m), 865 (w), 847 (w), 783 (m), 696 (w), 678 (w), 654 (w).

2.4. Gas Adsorption Measurements. The nitrogen adsorption experiment was performed at 77 K on a Micromeritics ASAP 2020 sorption analyzer after activation of the bulk sample at 50 °C for 10 h under primary vacuum. The desolvated sample was prepared as follows: A fresh sample was soaked in dimethylformamide (DMF) for 12 h, and the extract was discarded. Fresh DMF was subsequently added, and the sample was allowed to soak for another 12 h. The sample was then activation by flowing supercritical CO_2 more than 12 times. The measurement was maintained at 77 K with a liquid nitrogen bath.

2.5. Preparation of MOF Films. Substrates were cleaned with deionized water and acetone to remove impurities from the surface. Subsequently, the cleaned substrates were dried at 80 °C for 1 h before immersion in the mother solution. Additionally, the α-Al_2O_3 supports were activated for another 2 h at different temperature, such as 80, 120, and 160 °C before crystallization at 120 °C under solvent thermal conditions. A solid mixture of $Co(NO_3)_2{\cdot}6H_2O$ (0.2 mmol) and H_3TBTC (0.1 mmol) was dissolved in a mixture of 10 mL of 4:1:1 (volume ratio) DMF/EtOH/H_2O by strong stirring for 10 min at room temperature. To prevent precipitation on the surface of the

dx.doi.org/10.1021/la402012d | *Langmuir* 2013, 29, 8657−8664

planar support, the support was oriented 90° by a Teflon holder. The substrate and homemade Teflon holder were immersed in the prepared solution (10 mL) in a 23 mL Teflon-lined autoclave, heated in a convection oven at 120 °C for 72 h, and then cooled to room temperature. After it was cooled, the film was washed with ethanol and dried at atmosphere.

2.6. Organic Vapor Probe Experiments. The synthesized films were fixed on the homemade setup and then exposed to methanol, acetone, ethanol, acetonitrile, deionized water, dichloromethane, and pyridine vapor for several hours (see Figure S5 of the Supporting Information). The occurrences of the phenomenon were recorded by the optical camera (Canon Digital IXUS 9901S).

2.7. Molecular Storage and Transport Experiments. The films were placed in the methyl orange (MO) solution with a certain concentration of 4 mg/L for dynamic adsorption. The absorbance of the MO solution was detected by an UV−vis spectrophotometer every 48 h. The saturated adsorption of the sample was again dipped into the same amount of deionized water. The UV−vis spectrophotometer was used to record the absorbance of the water and quantitatively calculated the quantity of the released MO molecules.

3. RESULTS AND DISCUSSION

Compound **1** was synthesized by the reaction of $Co(NO_3)_2{\cdot}6H_2O$ and H_3TBTC at 120 °C under solvent thermal conditions. Single-crystal XRD analysis reveals that complex **1** crystallizes in space group $P\bar{1}$. The asymmetric unit contains two crystallographically independent Co^{II}, one $TBTC^{3-}$ (Figure 1a and see Figure S1a of the Supporting Information) and one coordinated DMF molecule. The two crystallographically independent Co^{II} ions have different coordination environments (Figure 1b). Co1, having an octahedral coordination environment, is bound to six oxygen atoms from six $TBTC^{3-}$, whereas Co2 is coordinated by four carboxylate oxygen atoms from three $TBTC^{3-}$ ligands and one oxygen atom from the DMF molecule, giving a highly distorted trigonal bipyramidal coordination geometry. Each Co1 links two Co2 by the $TBTC^{3-}$ ligand into a trimetallic cluster. Each cluster connects six $TBTC^{3-}$ ligands, and each $TBTC^{3-}$ ligand binds three clusters to form a two-dimensional (2D) (3,4)-connected net (Figure 1c). The adjacent 2D layers are packed together and stabilized by hydrogen bonds and $\pi-\pi$ interactions (Figure 1d). A view along the *a* axis shows one-dimensional (1D) channels beween the 2D layers with sizes of 15.4 × 8.5 Å (see Figure S1b of the Supporting Information). The potential solvent-accessible volume in compound **1** is estimated to be 35.6% by PLATON (free-guest removal).

The thermal stability of compound **1** was studied by TGA. The thermogravimetry (TG) curve shows two weight losses (see Figure S3 of the Supporting Information): the first weight loss of 17.5% in the range of 30−200 °C is related to the loss of DMF molecules (calculated at 16.7%), and the second weight loss of 41% between 260 and 470 °C is contributable to the decomposition of the compound.

The permanent porosity of the desolvated sample was confirmed by the N_2 sorption experiment at 77 K. As shown in Figure 2, the N_2 adsorption isotherm of compound **1** reveals typical type-IV behavior, as expected for a microporous material. Application of the standard Brunauer−Emmett−Teller (BET) model for N_2 adsorption gives a surface area of 615.03 m^2/g for compound **1**. The pore volume of 0.096 cm^3/g is calculated using the *t*-plot method with the Harkins and Jura model. Additionally, the N_2 sorption isotherm of compound **1** exhibits a hysteretic phenomenon on the desorption branch with an equilibrium time of 5 s during the measurement. The behavior is most likely resulting from the porous structure with

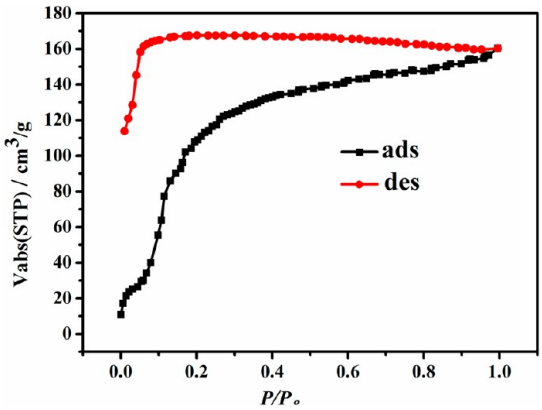

Figure 2. Gas sorption isotherm of N_2 at 77 K. ads, adsorption; des, desorption.

small openings connecting large cavities, leading to the formation of a strong interaction between porous and gas molecules at low temperatures.[33−35]

Subsequently, compound **1** was successfully deposited on α-Al_2O_3. It is well-known that substrate surface properties play an important role in the interface growth.[36] Besides, the MOFs based on flexible ligands are sensitive to many subtle factors. Keeping this in mind, before dipping the substrates into the mother solution at 120 °C for solvent thermal growth of compound **1**, the activation of substrates was performed under various temperatures. SEM confirms that the pre-activation temperature is the key factor to the morphology of the films. As shown in Figure 3, it is found that the films on supports

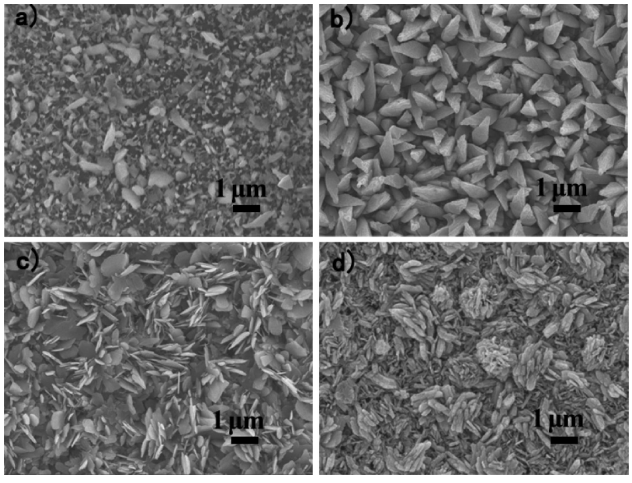

Figure 3. SEM images of the films induced by different pre-activation temperatures of alumina under the same solvent thermal conditions: (a) non-activated alumina, (b) alumina activated at 80 °C atmosphere, (c) alumina activated at 120 °C atmosphere, and (d) alumina activated at 160 °C atmosphere.

activated at different temperatures exhibit different scales of microcrystals: i.e., the grain size on the film is about 400 nm with a taper shape if the alumina is activated at 80 °C; when the substrate is activated at 120 °C, the sheet shape of about 80 nm microcrystals is observed; and the thin plate shape with a grain size of about 135 nm forms on the substrate activated at 160 °C. XRD patterns of the films are in good agreement with the simulated pattern from single-crystal data (Figure 4). It was reported that hot treatment would enhance surfactivity of

dx.doi.org/10.1021/la402012d | *Langmuir* 2013, 29, 8657−8664

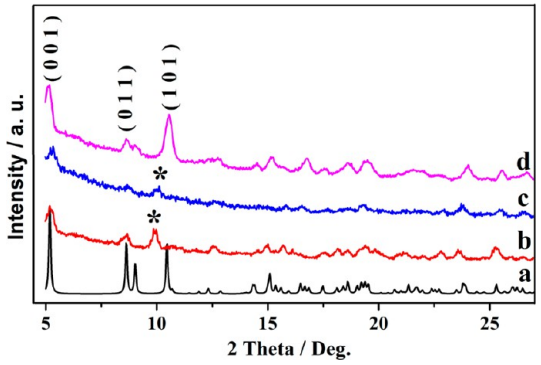

Figure 4. XRD data of $[Co_3(TBTC)_2{\cdot}(DMF)_2]{\cdot}4DMF$ thin films on α-Al_2O_3 growth from different pre-activation temperature supports: (a) simulated curved, (b) 80 °C, (c) 120 °C, and (d) 160 °C. "*" represents the peak of α-Al_2O_3. Each pattern is normalized to the most intense reflection.

alumina and, thus, increase the number of hydrogen bonds between α-Al_2O_3 supports and ligands, which could accelerate the heterogeneous nucleation.[37−39] Our results indicate that the pre-activation temperature of substrates may alter the compactness of hydroxyl groups on the surface of α-Al_2O_3, which leads to the improvement of the nucleating density. Accordingly, it may affect the shapes of microcrystals and grain sizes on α-Al_2O_3 supports.

On the other hand, the porous MOFs based on a flexible H_3TBTC ligand are different from those constructed by rigid ligands.[9−21] For different fabricating factors, the H_3TBTC ligand may adopt different conformations to interface with substrates before coordinating with metal ions. As highlighted in panels b and c of Figure 3, the morphology of the films displays a taper shape and sheet fashion, respectively. Tuning the pre-activation temperature of substrates, the target morphology can be acquired.

The film induced by non-actived α-Al_2O_3 substrate was also studied by SEM. In comparison to the preceding results, this film is less dense and discontinuous (Figure 3a). The probable reason is that only a small number of free hydroxyl groups arrange irregular on the non-activated α-Al_2O_3 surface, leading to growth of the disordered film.

Nucleation and growth may take place in the interface between the solid support and the bulk solution. The crystals grow by consuming the underlying Co^{2+} and $TBTC^{3-}$ ligands after nucleation on the substrate surface. To better understand the formation mechanism of the films on supported α-Al_2O_3 substrates, different amounts of the reactants were adopted to carry out the experiments. All films were fabricated under 120 °C solvent thermal condition. It is found that the growth of films depends upon the dosage of reactants to a certain extent. SEM was used to monitor the surface morphology of the MOF films prepared from mother solutions of different amounts of reactants. Through the SEM images, we can recognize the nucleation and growth between solid support and bulk solution well. As shown in Figure 5a, the defects can be observed from the top view. With the increase of the dosages of reactant, the films become denser and more uniform (panels b−d of Figure 5). The observation suggests that nucleation is an activated process, and the growing nuclei must overcome an energy barrier.[40,41] Because the critical nuclei have a high free energy, the nuclei either become inactivated or grow into crystals once they formed. The dilute solution cannot provide sufficient

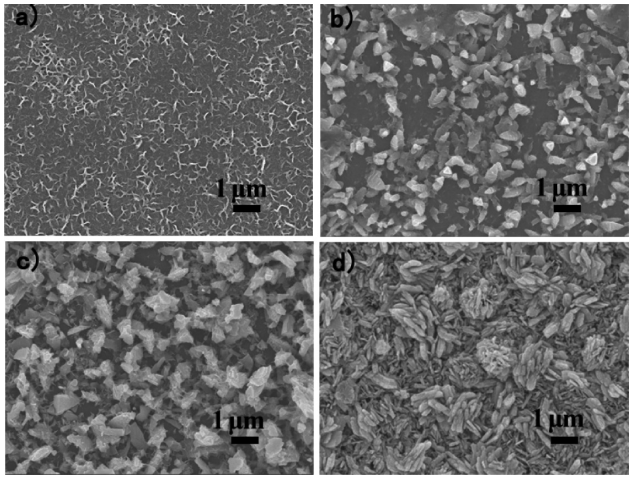

Figure 5. SEM images of the films of different usages of reactant: (a) 0.029 mmol of Co^{2+} and 0.014 mmol of $TBTC^{3-}$, (b) 0.04 mmol of Co^{2+} and 0.02 mmol of $TBTC^{3-}$, (c) 0.067 mmol of Co^{2+} and 0.033 mmol of $TBTC^{3-}$, and (d) 0.2 mmol of Co^{2+} and 0.1 mmol of $TBTC^{3-}$.

nutrition, leading the nuclei unable to grow effectively and simultaneously on the surface. Consequently, the morphology of the film exhibits irregular at a low-dosage concentration. With the increase of the amount of metal ions and ligands, the solution provides more nutrition for the growth of crystals, promoting the nuclei epitaxial growth on the surface.

ATR−IR also confirms the formation of the films (Figure 6). As shown in Figure 6, the curves of the films are consistent with

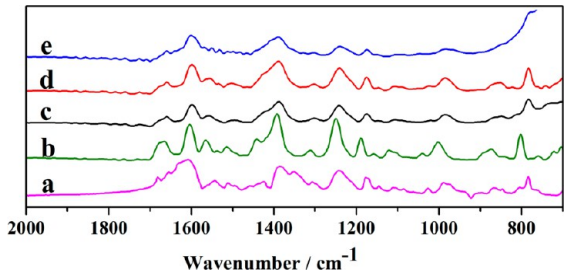

Figure 6. ATR−IR of $[Co_3(TBTC)_2{\cdot}(DMF)_2]{\cdot}4DMF$ thin films on α-Al_2O_3 growth from different concentractions: (a) bulk crystal, (b) 0.20 mmol of Co^{2+} and 0.1 mmol of $TBTC^{3-}$, (c) 0.067 mmol of Co^{2+} and 0. 033 mmol of $TBTC^{3-}$, (d) 0.04 mmol of Co^{2+} and 0.02 mmol of $TBTC^{3-}$, and (e) 0.029 mmol of Co^{2+} and 0.014 mmol of $TBTC^{3-}$.

the bulk powder. ATR−IR intensity of the films significantly increases with the reactants increasing. The characteristic peak at 1601 cm^{-1} is mainly assigned to the carboxyl groups. The peaks at 1390, 1239, 1175, and 983 cm^{-1} belong to the stretching vibration of Ar−O−CH_2. The peaks at 774 cm^{-1} can be attributed to vibrations of benzene rings.

As a representative example, the film that grows at the dosage of 0.2 mmol of Co^{2+}/0.1 mmol of $TBTC^{3-}$ is depicted here in detail. The SEM image of the MOF film on the solid surface is presented in Figure 5d. The result reveals that a continuous and rough film is formed on the solid−liquid interface. The grain size of compound **1** on the film is less than 1 μm. The crystal shape, analogous to lamellar, is controllable. From the cross-section view (Figure 7), it can be seen that the thickness of the film is about 580 nm. The grain size is in the nanoscale scope (Figure 5d). From this perspective, we can call the film as

dx.doi.org/10.1021/la402012d | *Langmuir* 2013, 29, 8657−8664

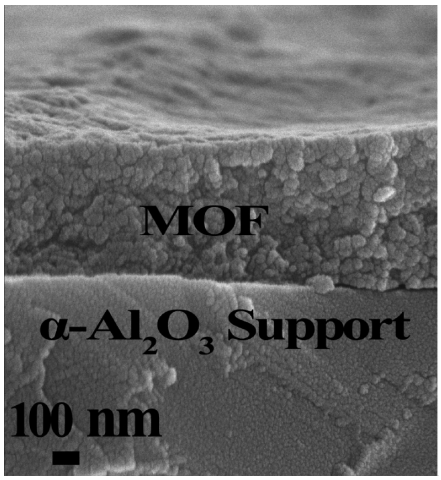

Figure 7. Cross-section view of $[Co_3(TBTC)_2\cdot(DMF)_2]\cdot 4DMF$ films growth at the dosage of 0.2 mmol of Co^{2+}/0.1 mmol of $TBTC^{3-}$.

flexible surface-mounted metal−organic frameworks[42] (F-SURMOFs).

In addition, the stretching OH vibration in infrared spectra was applied to characterize the free hydroxyl groups of the alumina surface (see Figure S4 of the Supporting Information). The OH groups are observed in the range of 3200−3900 cm^{-1}. Assignments are consistent with the result reported in the literature.[43,44] Thus, surface grown can be assumed that carboxyl groups of $TBTC^{3-}$ bond with hydroxyl groups by hydrogen bonding on the support surface before the growth of compound **1**[45] (Figure 8). In fact, alumina itself presents a high

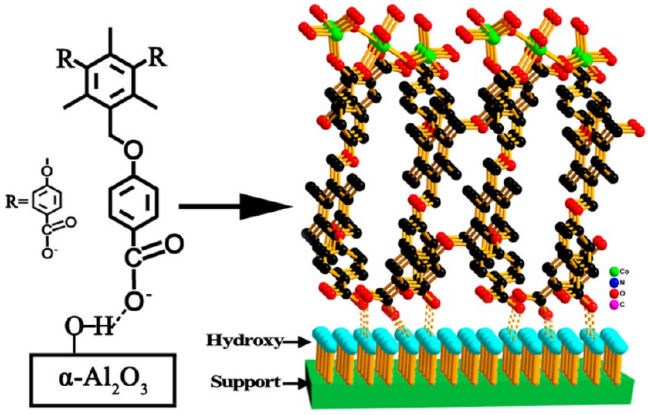

Figure 8. Possibility growth of compound **1** on α-Al_2O_3.

affinity for carboxylic groups.[46,47] Besides, to pre-activate substrate as well as to cool the growth solution slowly would enhance secondary bonding, such as hydrogen bonding or van der Waals interactions formed.[48]

The extraordinary properties of the films were also studied. Samples were exposed to the saturated methanol, acetone, ethanol, acetoneitrile, deionized water, dichloromethane, and pyridine vapor for several hours. The color of films changes obviously and quickly when exposed in methanol and pyridine vapor but no obvious change in other solvent vapor (Figure 9). The most noticeable feature is that the color can be recovered if the films exposed to methanol vapor previously are again dipped into the saturated DMF vapor. However, the films exposed to the pyridine cannot recover at room temperature. When the sample exposed in pyridine atmosphere was heated for several minutes in DMF atmosphere, the color can recover to the original color. The visual and direct sensing behaviors of the films imply that these films can be applied to distinguish methanol from pyridine or other molecules quickly.

When methanol and pyridine molecules were exchanged with the solvent molecules of compound **1**, the host framework may be changed simultaneously, as shown in Figures S6 and S12 of the Supporting Information, which may affect the local coordination environment of cobalt ions in compound **1**. As previous reported, compounds with varied cobalt coordination environments can display different colors.[49−51] Intrinsically, the $-O-CH_2-$ moieties in H_3TBTC may endow the ligand certain flexibility, and the ligand flexibility favors the framework transformation.[25,28,50] Consequently, the host framework of compound **1** can adopt its structure according to the size, shape, and interaction fashions of the guests being exchanged[52,53] Hence, the films can show a specific color response to methanol and pyridine sensitively. The methanol-exchanged compound **1** was described as **1**·MeOH, and the pyridine-exchanged compound **1** was denoted as **1**·pyridine.

The structure of compound **1** has changed upon the guest exchange in methanol atmosphere (see Figure S6b of the Supporting Information). Because of the different size and shape of methanol and DMF molecules, the framework of compound **1** may adjust slightly, while DMF molecules are substituted by methanol molecules. The color change from deep blue to pink is observed during the guest exchange process (Figure 9), which is likely responsible for the change of the cobalt coordination environment.[49−51] Moreover, the color change caused by DMF/MeOH guest exchange is reversible by simply repeating the process with the MeOH-containing sample in DMF atmosphere. The result indicates that the DMF guest molecules existing in channels of compound **1** can be exchanged by MeOH reversibly, accompanied by a detectable color change. Framework flexibility is believed to be a key reason for the reversible guest exchange and color change via a slight change of the coordination environment around metal centers (see Figure S6c of the Supporting Information). The behavior suggests that the film based on compound **1** as a sensor can be used effectively and cyclically.

FTIR spectra were also used to confirm the changes of compound **1** being exposed in methanol vapor. In the FTIR spectra (see Figure S7b of the Supporting Information), the characteristics at 1657 cm^{-1} ascribed to the C═O bending vibration of DMF disappear after exposure of compound **1** in methanol. The peak at 1681 cm^{-1} corresponding to $\nu_{C=O}$ of Ar−C═O of the ligand is vanished as well. Inversely, the peaks appear again in the infrared spectra recorded with samples of **1**·MeOH exposed in DMF atmosphere (see Figure S7c of the Supporting Information). The ^1H NMR spectra also indicate that the methanol molecules are trapped in the channels with approximately 2 methanol molecules per $TBTC^{3-}$ ligand (see Figure S8 of the Supporting Information). When **1**·MeOH is exposed in DMF atmosphere again, the ^1H NMR spectra show 3 DMF molecules per $TBTC^{3-}$ ligand (see Figure S9 of the Supporting Information), which is good agreement with the numbers calculated from TGA measurements (see Figures S10 and S11 of the Supporting Information).

Upon exposure in pyridine vapor, the host framework of compound **1** adjusts its structure during the solvent exchange (see Figure S12b of the Supporting Information). The characteristics at 1665 cm^{-1} ascribed to the N−H vibration

dx.doi.org/10.1021/la402012d | Langmuir 2013, 29, 8657−8664

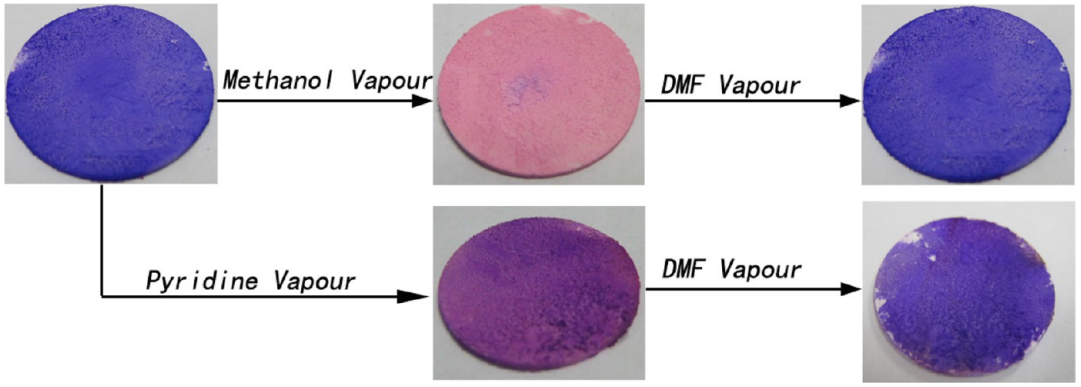

Figure 9. Optical photographs of film for the organic solvent vapor sensor.

of pyridine are observed in the FTIR spectra of **1**·pyridine. Simultaneously, the C═O stretching vibration of Ar−C═O of the ligand at 1681 cm^{-1} and the C═O bending vibration of DMF at 1657 cm^{-1} are vanished (see Figure S13b of the Supporting Information). The results confirm that the host framework has made configuration transition after incorporating pyridine. The changes of the framework may further affect the cobalt coordination environment, resulting in the deep blue color of compound **1** changing to purplish red. ^{1}H NMR spectra (see Figure S14 of the Supporting Information) and TGA (see Figure S16 of the Supporting Information) also confirm that pyridine has replaced DMF in the channels of compound **1**.

Unlike in the DMF/MeOH exchange, the color change from dark blue to purplish red observed in DMF/pyridine exchange is not reversible at room temperature. It is presumable that the host framework of compound **1** may form strong $\pi-\pi$ interactions with pyridine molecules.[52,53] However, the purplish red **1**·pyridine shows a color change back to deep blue when heating in DMF for several minutes. The XRD and FTIR spectra confirm that the structure of **1**·pyridine has changed back to the original (see Figures S12c and S13c of the Supporting Information). The ^{1}H NMR spectra show 3 DMF molecules per $TBTC^{3-}$ ligand (see Figure S15 of the Supporting Information). The behavior is identified by TGA as well (see Figure S17 of the Supporting Information).

In other words, flexible H_3TBTC allows for the host framework to adjust the structure quickly as long as the different guest molecules are exchanged.[54,55] Interestingly, a reversible color change can be observed during the solvent-exchange process (upon heating for pyridine/DMF exchange). The "reversible" color change shown by the solvated sample **1** is most likely attributed to the change of the cobalt coordination environment resulted from the flexible $-CH_2-O-$ moieties of H_3TBTC.

Meaningfully, the films are sensitive to the small dye molecule MO (Figure 10). The absorbance is significantly reduced while the thin films dipped in MO solution with time, exhausting at a certain concentration (Figure 10a). The reason is that the film can adsorb the MO molecules. The C−O−C and C═O moieties of flexible H_3TBTC may form a hydrogen bond or van der Waals interaction with the terminal group of the MO molecules. Besides, the MO molecules may come into the three-dimensional (3D) channel of the MOF. More interesting, the MO molecules can release to the fresh water slowly if the adsorption equilibrium sample is put back into the deionized water (Figure 10b). The most likely is the presence

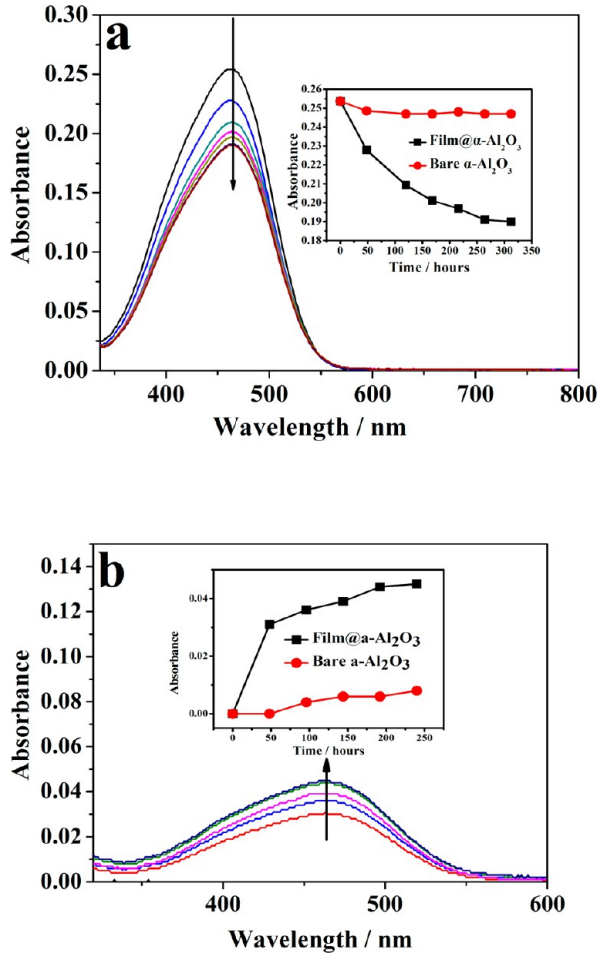

Figure 10. UV−vis spectra of the MO (4 mg/L) after (a) adsorption and (b) release (Inset) Maximum absorbance at 463 nm as a function of hours.

of Brownian movement. Some MO molecules on the surface of the MOF film or on the grains gap can release to the water under molecular collision. However, the MO molecules in the channel of the MOF will not be easy to come out to the water. Therefore, the transfer efficiency cannot be absolute. This behavior implies that these F-SURMOFs have potentially profound impacts on the storage and release of certain molecules.

dx.doi.org/10.1021/la402012d | *Langmuir* 2013, 29, 8657−8664

CONCLUSION

In summary, compound **1** was prepared using a flexible tricarboxylate ligand H_3TBTC under solvent thermal conditions. Subsequently, compound **1** is fabricated as a film on α-Al_2O_3 substrates. The films are sensitive to many subtle factors because of the flexibility of H_3TBTC. Tuning subtle factors of fabrication, a series of films with different morphologies and grain sizes can be obtained. The result indicates that the morphology and grain size can be controlled. Additionally, the morphology and grain size of films are also affected by the pre-activation temperature of substrates and the dosages of reagents. For a higher pre-activation temperature, the films can grow with a much denser morphology and much smaller grain size. With the increase of the dosages of the reagents, the films can be much denser and more uniform. Furthermore, the $-CH_2-O-$ moieties of flexible H_3TBTC can allow for the host framework to adjust the structure flexibility as soon as the different guest molecules are incorporated by compound **1**. Meanwhile, the framework transition may affect the cobalt environment. Consequently, the films based on compound **1** can change color sensitively. The behavior of the films is expected to be promising in the applications of optical devices. Moreover, the adsorption and liberation of MO by the films have a profound effect on molecule storage and release.

ASSOCIATED CONTENT

Supporting Information

Synthesis of the ligand, simplified representation of the geometry of the ligand in compound **1**, 2D layer extended structure of guest-free, ^{1}H NMR spectra of the ligand, and ATR–IR spectra of alumina disc. This material is available free of charge via the Internet at http://pubs.acs.org.

AUTHOR INFORMATION

Corresponding Author

*Telephone/Fax: +86-591-83796710. E-mail: rcao@fjirsm.ac.cn.

Notes

The authors declare no competing financial interest.

ACKNOWLEDGMENTS

We thank the 973 Program (2011CB932504 and 2012CB821705), the National Natural Science Foundation of China (NSFC) (21221001, 20901078, and 21173222), the Fujian Key Laboratory of Nanomaterials (2006L2005), the Key Project from the Chinese Academy of Science (CAS).

REFERENCES

(1) Jiang, H. L.; Xu, Q. Porous metal–organic frameworks as platforms for functional applications. *Chem. Commun.* **2011**, *47*, 3351–3370.

(2) Long, J. R.; Yaghi, O. M. The pervasive chemistry of metal–organic frameworks. *Chem. Soc. Rev.* **2009**, *38*, 1203–1212.

(3) Kuppler, R. J.; Timmons, D. J.; Fang, Q. R.; Li, J. R.; Makal, T. A.; Young, M. D.; Yuan, D. Q.; Zhao, D.; Zhuang, W. J.; Zhou, H. C. Potential applications of metal–organic frameworks. *Coord. Chem. Rev.* **2009**, *253*, 3042–3066.

(4) Keskin, S.; Sholl, D. S. Efficient methods for screening of metal organic framework membranes for gas separations using atomically detailed models. *Langmuir* **2009**, *25*, 11786–11795.

(5) Byrd, H.; Holloway, C. E.; Pogue, J.; Kircus, S.; Advincula, R. C.; Knoll, W. Ultrathin film self-assembly of hybrid organic–inorganic metal coordination polymers. *Langmuir* **2000**, *16*, 10322–10328.

(6) Belghoul, B.; Welterlich, I.; Maier, A.; Toutianoush, A.; Rabindranath, A. R.; Tieke, B. Supramolecular sequential assembly of polymer thin films based on dimeric, edndrimeric, and polymeric Schiff-base ligands and metal ions. *Langmuir* **2007**, *23*, 5062–5069.

(7) Gao, S. Y.; Zheng, Z. L.; Lü, J.; Cao, R. Progressive release of a palladium–pyridyl complex from a layer-by-layer multilayer and illustrative application to catalytic Suzuki coupling. *Chem.Commun.* **2010**, *46*, 7584–7586.

(8) Gao, S. Y.; Huang, Y. B.; Cao, M. N.; Liu, T. F.; Cao, R. The fabrication of palladium–pyridyl complex multilayers and their application as a catalyst for the Heck reaction. *J. Mater. Chem.* **2011**, *21*, 16467–16472.

(9) Tavolaro, A.; Drioli, E. Zeolite membrances. *Adv. Mater.* **1999**, *11*, 975–996.

(10) Bétard, A.; Fischer, R. A. Metal–organic framework thin films: From fundamentals to applications. *Chem. Rev.* **2012**, *112*, 1055–1083.

(11) Gascon, J.; Kapteijn, F.; Zornoza, B.; Sebastián, V.; Casado, C.; Coronas, J. Practical approach to zeolitic membranes and coatings: State of the art, opportunities, barriers, and future perspectives. *Chem. Mater.* **2012**, *24*, 2829–2844.

(12) Hermes, S.; Schröder, F.; Chelmowski, R.; Wöll, Ch.; Fischer, R. A. Selective nucleation and growth of metal–organic open framework thin films on patterned COOH/CF_3-terminated self-assembled monolayers on Au(111). *J. Am. Chem. Soc.* **2005**, *127*, 13744–13745.

(13) Hermes, S.; Zacher, D.; Baunemann, A.; Wöll, Ch.; Fischer, R. A. Selective growth and MOCVD loading of small single crystals of MOF-5 at alumina and silica surfaces modified with organic self-assembled monolayers. *Chem. Mater.* **2007**, *19*, 2168–2173.

(14) Yoo, Y.; Jeong, H.-K. Rapid fabrication of metal organic framework thin films using microwave-induced thermal deposition. *Chem. Commun.* **2008**, 2441–2443.

(15) Liu, Y.; Ng, Z.; Khan, E. A.; Jeong, H. K.; Ching, C. B.; Lai, Z. Synthesis of continuous MOF-5 membranes on porous α-alumina substrates. *Microporous Mesoporous Mater.* **2009**, *118*, 296–301.

(16) Guo, H.; Zhu, G. S.; Hewitt, L. J.; Qiu, S. L. "Twin copper source" growth of metal–organic framework membrane: $Cu_3(BTC)_2$ with high permeability and selectivity for recycling H_2. *J. Am. Chem. Soc.* **2009**, *131*, 1646–1647.

(17) Zacher, D.; Baunemann, A.; Hermes, S.; Fischer, R. A. Deposition of microcrystalline $[Cu_3(btc)_2]$ and $[Zn_2(bdc)_2(dabco)]$ at alumina and silica surfaces modified with patterned self assembled organic monolayers: Evidence of surface selective and oriented growth. *J. Mater. Chem.* **2007**, *17*, 2785–2792.

(18) Shekhah, O.; Wang, H.; Kowarik, S.; Schreiber, F.; Paulus, M.; Tolan, M.; Sternemann, C.; Evers, F.; Zacher, D.; Fischer, R. A.; Wöll, Ch. Step-by-step route for the synthesis of metal–organic frameworks. *J. Am. Chem. Soc.* **2007**, *129*, 15118–15119.

(19) Keskin, S.; Liu, J. C.; Johnson, J. K.; Sholl, D. S. Testing the accuracy of correlations for multicomponent mass transport of adsorbed gases in metal–organic frameworks: Diffusion of H_2/CH_4 mixtures in CuBTC. *Langmuir* **2008**, *24*, 8254–8261.

(20) Keskin, S.; Liu, J. C.; Johnson, J. K.; Sholl, D. S. Atomically-detailed models of gas mixture diffusion through CuBTC membrances. *Microporous Mesoporous Mater.* **2009**, *25*, 11786–11795.

(21) Ameloot, R.; Stappers, L.; Fransaer, J.; Alaerts, L.; Sels, B. F.; De Vos, D. E. Patterned growth of metal–organic framework coatings by electrochemical synthesis. *Chem. Mater.* **2009**, *21*, 2580–2582.

(22) Hu, Y. X.; Dong, X. L.; Nan, J. P.; Jin, W. Q.; Ren, X. M.; Xu, N. P. Metal–organic framework membranes fabricated via reactive seeding. *Chem. Commun.* **2011**, *47*, 737–739.

(23) Centrone, A.; Yang, Y.; Speakman, S.; Bromberg, L.; Rutledge, G. C.; Hatton, T. A. Growth of metal–organic frameworks on polymer surfaces. *J. Am. Chem. Soc.* **2010**, *132*, 15687–15691.

(24) Scherb, C.; Schödel, A.; Bein, T. Directing the structure of metal–organic frameworks by oriented surface growth on an organic monolayer. *Angew. Chem., Int. Ed.* **2008**, *47*, 5777–5779.

(25) Zhang, C. J.; Su, C. Coordination assemblies of metallacyclic, prismatic and tubular molecular architectures based on the non-rigid ligands. *Eur. J. Inorg. Chem.* **2007**, 2997–3010.

(26) Rabone, J.; Yue, Y. F.; Chong, S. Y.; Stylianou, K. C.; Bacsa, J.; Bradshaw, D.; Darling, G. R.; Berry, N. G.; Khimyak, Y. Z.; Ganin, A. Y.; Wiper, P.; Claridge, J. B.; Rosseinsky, M. J. An adaptable peptide-based porous material. *Science* **2010**, *329*, 1053−1057.
(27) Dong, B. X.; Xu, Q. Investigation of flexible organic ligands in the molybdate system: Delicate influence of a peripheral cluster environment on the isopolymolybdate frameworks. *Inorg. Chem.* **2009**, *48*, 5861−5873.
(28) Liu, T. F.; Lü, J.; Shi, L. X.; Guo, Z. G.; Cao, R. Conformation control of a flexible 1,4-phenylenediacetate ligand in coordination complexes: A rigidity-modulated strategy. *Cryst. Eng. Comm.* **2009**, *11*, 583−588.
(29) Guo, Z. G.; Cao, R.; Wang, X.; Li, H. F.; Yuan, W. B.; Wang, G. J.; Wu, H. H.; Li, J. A multifunctional 3D ferroelectric and NLO-active porous metal−organic framework. *J. Am. Chem. Soc.* **2009**, *131*, 6894−6895.
(30) Liu, T. F.; Lü, J.; Lin, X.; Cao, R. Construction of a trigonal bipyramidal cage-based metal−organic framework with hydrophilic pore surface via flexible tetrapodal ligands. *Chem. Commun.* **2010**, *46*, 8439−8441.
(31) Lin, Z. J.; Liu, T. F.; Huang, Y. B.; Lü, J.; Cao, R. A guest-dependent approach to retain permanent pores in flexible metal−organic frameworks by cation exchange. *Chem.—Eur. J.* **2012**, *18*, 7896−7902.
(32) Oike, H.; Imamura, H.; Imaizumi, H.; Tezuka, Y. Tailored synthesis of branched and network polymer structures by electrostatic self-assembly and covalent fixation with telechelic poly(THF) having *N*-phenylpyrrolidinium salt groups. *Macromolecules* **1999**, *32*, 4819−4825.
(33) Zhao, D.; Yuan, D. Q.; Krishna, R.; Baten, J. M.; van, B.; Zhou, H. C. Thermosensitive gating effect and selective gas adsorption in a porous coordination nanocage. *Chem. Commun.* **2010**, *46*, 7352−7354.
(34) Liu, T. F.; Chen, Y. P.; Yakovenko, A. A.; Zhou, H. C. Interconversion between discrete and a chain of nanocages: Self-assembly via a solvent-driven, dimension-augmentation strategy. *J. Am. Chem. Soc.* **2012**, *134*, 17358−17361.
(35) Zhang, J. P.; Chen, X. M. Exceptional framework flexibility and sorption behavior of a multifunctional porous cuprous triazolate framework. *J. Am. Chem. Soc.* **2008**, *130*, 6010−6017.
(36) Jiang, D. M.; Burrows, A. D.; Jaber, R.; Edler, K. J. Facile synthesis of metal−organic framework films via *in situ* seeding of nanoparticles. *Chem. Commun.* **2012**, *48*, 4965−4967.
(37) Yoo, Y.; Varela-Guerrero, V.; Jeong, H.-K. Isoreticular metal−organic frameworks and their membranes with enhanced crack resistance and moisture stability by surfactant-assisted drying. *Langmuir* **2011**, *27*, 2652−2657.
(38) Demessence, A.; Horcajada, P.; Serre, C.; Boissière, C.; Grosso, D.; Sanchez, C.; Férey, G. Elaboration and properties of hierarchically structured optical thin films of MIL-101(Cr). *Chem. Commun.* **2009**, 7149−7151.
(39) Southon, P. D.; Liu, L.; Fellows, E. A.; Price, D. J.; Halder, G. J.; Chapman, K. W.; Moubaraki, B.; Murray, K. S.; Létard, J. F.; Kepert, C. J. Dynamic interplay between spin-crossover and host−guest function in a nanoporous metal−organic framework material. *J. Am. Chem. Soc.* **2009**, *131*, 10998−11009.
(40) Sear, R. P. Nucleation: Theory and applications to protein solutions and colloidal suspensions. *J. Phys.: Condens. Matter* **2007**, *19*, 033101−033129.
(41) Li, S. Z.; Shi, W. X.; Lu, G.; Li, S. Z.; Loo, S. C. J.; Huo, F. W. Unconventional nucleation and oriented growth of ZIF-8 crystals on non-polar surface. *Adv. Mater.* **2012**, *24*, 5954−5958.
(42) Shekhah, O. Layer-by-layer method for the synthesis and growth of surface mounted metal−organic frameworks (SURMOFs). *Materials* **2010**, *3*, 1302−1315.
(43) El-Nadjar, W.; Bonne, M.; Trela, E.; Rouleau, L.; Mino, A.; Hocine, S.; Payen, E.; Lancelot, C.; Lamonier, C.; Blanchard, P.; Courtois, X.; Can, F.; Duprez, D.; Royer, S. Infrared investigation on surface properties of alumina obtained using recent templating routes. *Microporous Mesoporous Mater.* **2012**, *158*, 88−98.
(44) Lorite, I.; Martín-González, M. S.; Romero, J. J.; García, M. A.; Fierro, J. L. G.; Fernández, J. F. Electrostatic charge dependence on surface hydroxylation for different Al_2O_3 powders. *Ceram. Int.* **2012**, *38*, 1427−1434.
(45) Truter, L. A.; Ordomsky, V. V.; Nijhuis, T. A.; Schouten, J. C. Preparation of ZSM-5 zeolite coatings within capillary microchannels. *J. Mater. Chem.* **2012**, *22*, 15976−15980.
(46) Allara, D. L. Spontaneously organized molecular assemblies. 1. Formation, dynamics, and physical properties of *n*-alkanoic acids adsorbed from solution on an oxidized aluminum surface. *Langmuir* **1985**, *1*, 45−52.
(47) Chen, S. H.; Frank, C. W. Infrared and fluorescence spectroscopic studies of self-assembled *n*-alkanoic acid monolayers. *Langmuir* **1989**, *5*, 978−987.
(48) Huang, A.; Dou, W.; Caro, J. Steam-stable zeolitic imidazolate framework ZIF-90 membrane with hydrogen selectivity through covalent functionalization. *J. Am. Chem. Soc.* **2010**, *132*, 15562−15564.
(49) Chen, C. L.; Goforth, A. M.; Smith, M. D.; Su, C. Y.; Loye, H. C. $[Co_2(ppca)_2(H_2O)(V_4O_{12})_{0.5}]$: A framework material exhibiting reversible shrinkage and expansion through a single-crystal-to-single-crystal transformation involving a change in the cobalt coordination environment. *Angew. Chem., Int. Ed.* **2005**, *44*, 6673−6677.
(50) Chen, C. L.; Beatty, A. M. Guest inclusion and structural dynamics in 2-D hydrogen-bonded metal−organic framework. *J. Am. Chem. Soc.* **2008**, *130*, 17222−17223.
(51) Takaoka, K.; Kawano, M.; Tominaga, M.; Fujita, M. In situ observation of a reversible single-crystal-to-single-crystal apical-ligand-exchange reaction in a hydrogen-bonded 2D coordination network. *Angew. Chem., Int. Ed.* **2005**, *44*, 2151−2154.
(52) Wei, W.; L, W. L.; Li, Z. F.; Su, W. P.; Hong, M. C. Stabilization and controlled release of reactive molecules by solid-state van der Waals capsules. *Chem.—Eur. J.* **2013**, *19*, 469−473.
(53) Wei, W.; Wang, G.; Zhang, Y.; Jiang, F. L.; Wu, M. Y.; Hong, M. C. A versatile tripodal host with cylindrical conformation: Solvatomorphism, inclusion behavior, and separation of guests. *Chem.—Eur. J.* **2011**, *17*, 2189−2198.
(54) Férey, G.; Serre, C. Large breating effects in three-dimensional porous hybrid matter: Facts, analyses, rules and consequences. *Chem. Soc. Rev.* **2009**, *38*, 1380−1399.
(55) Yanai, N.; Kitayama, K.; Hijikata, Y.; Sato, H.; Matsuda, R.; Kubota, Y.; Takata, M.; Mizuno, M.; Uemura, T.; Kitagawa, S. Gas detection by structural variations of fluorescent guest molecules in a flexible porous coordination polymer. *Nat. Mater.* **2011**, *10*, 787−793.